CHEMISTRY OF MATERIALS

ARTICLE

pubs.acs.org/cm

Short-Range Layered A-Site Ordering in Double Perovskites $NaLaBB'O_6$ (B = Mn, Fe; B′ = Nb, Ta)

Walid Dachraoui,[†,⊥] Tao Yang,[‡,⊥] Chang Liu,[‡,§] Graham King,[∥] Joke Hadermann,[†] Gustaaf Van Tendeloo,[†] Anna Llobet,[∥] and Martha Greenblatt*[,‡]

[†]EMAT, University of Antwerp, Groenenborgerlaan 171, 2020 Antwerp, Belgium

[‡]Department of Chemistry and Chemical Biology, Rutgers, The State University of New Jersey, 610 Taylor Road Piscataway, New Jersey 08854-8087, United States

[§]State Key Laboratory of Inorganic Synthesis and Preparative Chemistry, College of Chemistry, Jilin University, Changchun 130012, People's Republic of China

[∥]Lujan Neutron Scattering Center, Los Alamos National Laboratory, MS H805, Los Alamos, New Mexico 87545, United States

Supporting Information

ABSTRACT: The new compounds $NaLaFeTaO_6$, $NaLaFeNbO_6$, $NaLaMnTaO_6$, and $NaLaMnNbO_6$ have been synthesized and characterized with a combination of transmission electron microscopy, X-ray powder diffraction (XRPD), neutron powder diffraction (NPD), and magnetization measurements. Through electron microscopy study, a local layered order of the A-cations has been detected without the typical occurrence of rock salt order at the B-cation site. Satellite reflections in the electron diffraction related to the local layered order are not visible on the XRPD or NPD patterns. The occurrence of local layered order is supported by pair distribution function analysis, which also reveals the presence of uncorrelated displacements of the Nb and Ta cations. The octahedra are tilted according to the system $a^-b^+a^-$, and the coordinates were refined from XRPD and NPD with a disordered cation distribution in the space group *Pnma*. The magnetic exchange interactions in $NaLaFeTaO_6$ and $NaLaFeNbO_6$ are antiferromagnetic, while they are ferromagnetic in $NaLaMnTaO_6$ and $NaLaMnNbO_6$. Long-range magnetic ordering is not observed down to 4 K for any of the compositions.

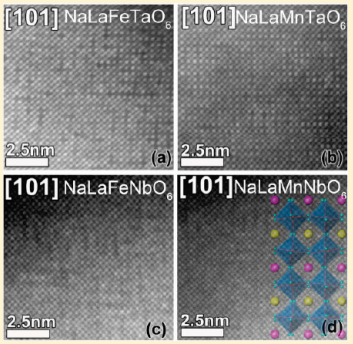

KEYWORDS: double perovskite, layered ordering, electron microscopy, magnetic

INTRODUCTION

The aristotype ABX_3 perovskite structure has a cubic unit cell, space group $Pm\bar{3}m$, with the A-cations located in the cuboctahedral centers created by the three-dimensional network of corner-sharing BO_6 octahedra. Cation order−disorder plays a critical role in the control of the crystal structure and the properties of many complex perovskite-type oxides. Superconductivity, colossal magnetoresistance, ferroelectricity, multiferroic behavior, magnetic ordering, piezoelectricity, and electronic and ionic conductivity strongly depend on the degree of order of the A- and/or B-sites.[1−4] The rock salt-type B-site ordering is the most commonly observed one, and over 400 examples have been reported.[5] Several comprehensive reviews about B-site ordering have been published.[6−8] Only a few Cu-based perovskites are demonstrated to have an unusual layer-by-layer ordering on the B-site: Ln_2CuSnO_6 (Ln = La, Pr, Nd, Sm), $La_{2-x}Sr_xCuSnO_6$ and La_2CuZrO_6.[9−11] Such unique layered ordering is believed to be driven by a strong first-order Jahn−Teller (FOJT) distortion of the CuO_6 octahedra, which results in four short in-plane Cu−O distances and two long apical ones nearly perpendicular to the (CuO_2) and (SnO_2) planes. Most recently, short-range layered ordering in perovskite $NaNb_{1-x}Ta_xO_3$ was surprisingly observed by electron microscopy.[12] The authors suggested that the only reasonable explanation for this unexpected ordering was the difference of electronegativity between Nb^{5+} and Ta^{5+}.

Moreover, layered ordering of the A-site cations among stoichiometric double perovskites has been observed in $NaLaBWO_6$ (B = Mg, Ni, Co, Mn), $NaLnMnWO_6$ (Ln = Ce, Pr, Nd, Sm, Gd, Dy, Ho), and $NaLnMgWO_6$ (Ln = Ce, Pr, Nd, Sm, Eu, Gd, Tb, Dy, Ho),[13] $NaLaScNbO_6$,[14] and $KLaMnWO_6$.[15] Several common features can be therefore found: A-sites are occupied by the alkaline metal Na (or K) and rare-earth elements with a charge difference of 2; in most cases the B-sites are occupied by bivalent cations and W^{6+} with the only exception of Sc^{3+} and Nb^{5+}. In a recent review,[16] it is concluded that A-site layered ordering is stabilized by the presence of a highly charged d^0 cation with second-order Jahn−Teller (SOJT) effect on one of the B-sites and also associated with B-site rock salt-type ordering, in the so-called "doubly-ordered" perovskites. It is very interesting that A-site layered and B-site rock salt orderings are synergistic,

Received: January 22, 2011
Revised: March 15, 2011
Published: April 14, 2011

and the removal of one leads to the disappearance of the other. One demonstration is the coupled orderings in $NaLaMgWO_6$, but the absence of A-site order in $NaLaTi_2O_6$. Moreover, it should be noted that several doubly ordered perovskites, $NaLaMnWO_6$, $NaNdMnWO_6$, and $NaTbMnWO_6$, adopt a noncentrosymmetric structure with $P2_1$ symmetry arising from the combination of the cation orderings and $a^-a^-c^+$ octahedral tilting.[15] Thus, the presence of both SOJT distortions of the d^0 cations and magnetic ions in such compounds potentially could lead to multiferroic behavior.

Examples of layered ordered A-site perovskites are relatively few. The above-mentioned B-site layered ordering of Ta^{5+} and Nb^{5+} in $NaNb_{1-x}Ta_xO_3$ and A-site layered ordering in $NaLaScNbO_6$, which is the only case without W^{6+} in the B-site, motivated us to explore $NaLaBB'O_6$ (B = Mn, Fe; B′ = Nb, Ta). The choice of cations with and without FOJT effect, Mn^{3+} and Fe^{3+}, together with Nb^{5+} and Ta^{5+}, with large differences of SOJT effect, allowed a systematic investigation presented here. Interestingly, all four perovskites show short-range layered A-site ordering, established by high-resolution transmission electron microscopy (HRTEM) and high-angle annular dark field STEM (HAADF-STEM). And importantly, the degree of the short-range ordering is, as expected, the highest in $NaLaMnNbO_6$ and the lowest in $NaLaFeTaO_6$, with the other two as intermediate. Detailed structural studies by X-ray/neutron powder diffraction (XRPD and NPD), total scattering, and electron microscopy (EM) are presented.

EXPERIMENTAL SECTION

$NaLaBB'O_6$ (B = Mn, Fe; B′ = Nb, Ta) were synthesized by conventional solid-state reactions in air. The starting materials, including La_2O_3 (obtained by the dehydration of $La(NO_3)_3 \cdot 6H_2O$ at 800 °C), Na_2CO_3 (Alfa Aesar, 99.997%), Mn_2O_3 (Aldrich, 99.999%)/Fe_2O_3 (Alfa Aesar, 99.99%), and Nb_2O_5 (Alfa, 99.9985%)/Ta_2O_5 (Aldrich, 99.99%), were ground thoroughly in a molar ratio Na:La:B:B′ = 1:1:1:1 in an agate mortar, pressed into a pellet, heated up to 1000 °C slowly, and maintained for 12 h. After this prereaction, the sample pellet was wrapped in Pt foil and further annealed at 1350 °C for 120 h with several intermediate regrindings. The purity of the products was confirmed by XRPD, which indicated no visible impurity reflection peaks.

XRPD data were recorded on a Bruker D8-Advance diffractometer (in Bragg−Brentano geometry with Cu Kα radiation, λ = 1.5406 Å, SOL-X solid state detector, 40 kV and 40 mA, step scan 10−120°/0.02°/15s). The refinements of the crystal structures from PXRD data was performed by the Rietveld method with the TOPAS software.[17]

Samples for electron microscopy were prepared by dispersing the powder in ethanol and depositing it on a holey carbon grid. Selected area electron diffraction (SAED) patterns were obtained on a Philips CM20 transmission electron microscope. HRTEM and HAADF-STEM were obtained with a Tecnai G2 transmission electron microscope. The composition of the samples was determined with energy dispersive X-ray (EDX) analysis performed with a JEOL JSM5510 scanning electron microscope on 50 crystallites for each sample; the Philips CM20 transmission electron microscope on each crystallite studied for electron diffraction, both instruments equipped with the Oxford INCA system.

The X-ray total scattering data used to obtain the pair distribution function was collected at the 11-BM beamline of the Advanced Photon Source at Argonne National Laboratory. The powder samples were loaded in capillaries. Data was collected on a flat plate detector with an X-ray wavelength of 0.1365 Å. The intensities of the powder diffraction rings were integrated with the program FIT2D.[18,19] Data reduction to obtain the $G(r)$ function was carried out with the program PDFgetX2.[20] The Q_{max} was 25 $Å^{-1}$ in all cases.

The neutron total scattering data used for Rietveld refinement and for pair distribution function analysis was collected on the HIPD instrument of the Lujan Neutron Scattering Center of Los Alamos National Laboratory. Data was collected at 300 and 4 K for each sample. Rietveld refinements were carried out with the GSAS/EXPGUI software package.[21,22] Reduction of the neutron data to obtain the pair distribution function, $G(r)$, was done with the program PDFgetN with a Q_{max} of 32 $Å^{-1}$.[23] Refinements of both the X-ray and neutron PDFs were done with the program PDFgui.[24] The following definition of the pair distribution function is used in this study: $G(r) = 4\pi r[\rho(r) - \rho_0]$, where $\rho(r)$ is the microscopic pair density, ρ_0 is the average pair density, and r is the radial distribution.

The dc magnetic susceptibility measurements were carried out on powder samples with a Quantum Design MPMS-XL superconducting quantum interference device (SQUID) magnetometer. Powder samples were placed in a gelatin capsule fastened in a plastic straw for immersion into the SQUID. Typical zero-field cooling (ZFC) and field-cooling (FC) magnetizations in the temperature range of 5−300 K were performed under external magnetic fields of 1 kOe. The isothermal magnetization curve was measured at 5 K up to 50 kOe.

RESULTS AND DISCUSSION

TEM Study. The compositions of the samples as measured by EDX analysis are $La_{1.0(1)}Na_xFe_{1.00(6)}Ta_{1.00(6)}O_y$, $La_{1.0(2)}Na_x$-$Mn_{0.94(12)}Ta_{1.06(12)}O_y$, $La_{1.0(4)}Na_xFe_{1.0(3)}Nb_{1.0(3)}O_y$, and $La_{1.0(2)}$-$Na_xMn_{0.94(12)}Nb_{1.06(12)}O_y$. The oxygen and sodium contents of these powder samples cannot be directly measured with EDX. All measured compositions are within the range of the nominal composition and for the remainder of the text they will be referred to by those nominal compositions.

SAED patterns were recorded from a large number of crystallites and zones of each sample; representative patterns of the four samples are shown in Figure 1. The patterns can all be indexed with unit cell parameters approximately $a = a_p\sqrt{2}$, $b = 2a_p$, $c = a_p\sqrt{2}$, where a_p is the unit cell parameter of the parent perovskite aristotype.

The reflections hkl: $h + k + l = 2n + 1$ are streaked when present, the hkl: $h + k + l = 2n$ reflections are not streaked. Because of the presence of 90° rotation twins, the streaked reflections are present in the [101] pattern along two perpendicular directions, and the [101] pattern is overlapping with the [010] pattern; the reflections at 1/2(oeo) (o = odd, e = even) in the [101] indexation shown on the pattern are therefore actually $h0l$: $h + l = 2n + 1$ reflections belonging to the [010] zone. Heating the samples inside the microscope does not reveal any changes in the ED patterns, which indicates that these streaks are not related to an incomplete phase transition.

To determine the origin of the streaked character of the hkl: $h + k + l = 2n + 1$ reflections, HRTEM and HAADF-STEM images were obtained. The contrast of HRTEM images is sensitive to structural modifications such as cation ordering, oxygen vacancies, and atomic displacements, even of oxygen positions. The contrast in a HAADF-STEM image is only negligibly influenced by the oxygen positions and is mainly dictated by the occupation of the cation columns. The higher the average Z of the column, the brighter the dot will be that represents that column; the brightness is related to the average Z along the atomic column as $\sim Z^n$ $(1.5 < n < 2)$.

dx.doi.org/10.1021/cm200226u |Chem. Mater. 2011, 23, 2398–2406

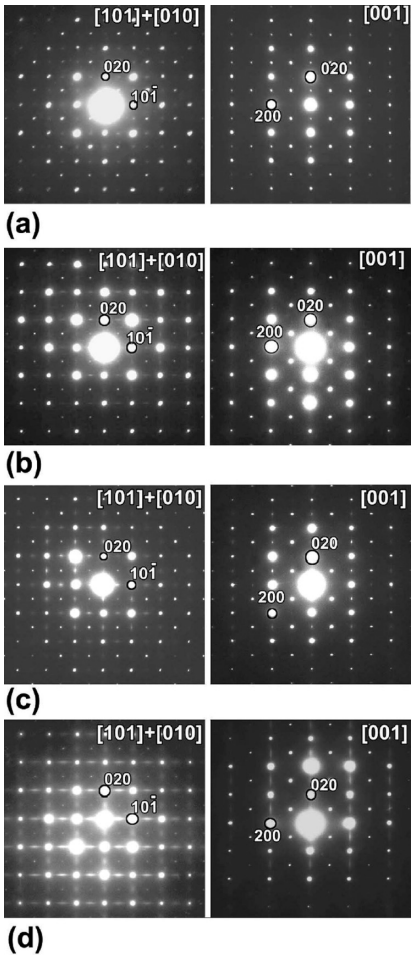

Figure 1. SAED patterns of the main zones of the four samples: (a) $NaLaFeTaO_6$, (b) $NaLaMnTaO_6$, (c) $NaLaFeNbO_6$, and (d) $NaLaMnNbO_6$. Reflection on [101] + [010] are indexed as in [101].

A HRTEM image of $NaLaFeNbO_6$ along $[101]_p$ (p refers to the perovskite subcell) is shown in Figure 2. In this HRTEM image the bright dots are associated with the cation positions. There are rows of less bright dots (indicated by white arrows) with a preferential periodicity equal to $b = 2a_p \approx 7.8$ Å. The HRTEM image does not, however, show unambiguously the reason for the contrast difference. Figure 3 shows the HAADF-STEM images for the four different compounds along that same $[101]_p$ direction. These images also locally show rows of darker dots, with a distance of approximately 7.8 Å between the rows. If the origin of the difference in brightness between the dots on the HRTEM image would be due to the tilting of octahedra, which is only a displacement of oxygen atoms, it would not have any effect on the HAADF-STEM images. Therefore, the brightness difference is attributed to a local ordering of the cations, more specifically, a layered order of either the A- or the B-cations. We can pinpoint which cations show the layered order by considering the average Z of the A and B columns for the compounds $NaLaFeTaO_6$ and $NaLaMnTaO_6$. In these compounds the average Z along the B-cation columns is much higher than that along the A-cation columns. Consequently, on the HAADF-STEM images of these two compounds the brighter dots belong to the projected B-cation columns. The alternation of brighter and darker rows of dots appears for the overall less

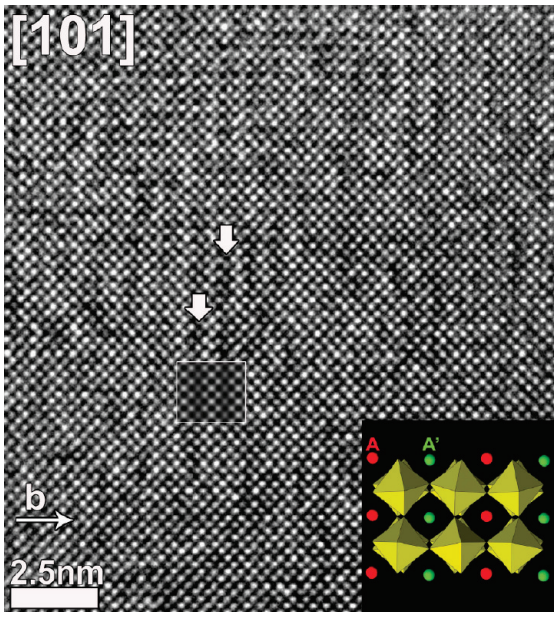

Figure 2. HRTEM image of $NaLaFeNbO_6$ along [101]. A calculated image is set in the experimental one and is indicated with a white border. A scheme of the model used for the calculated image is shown in the bottom right corner.

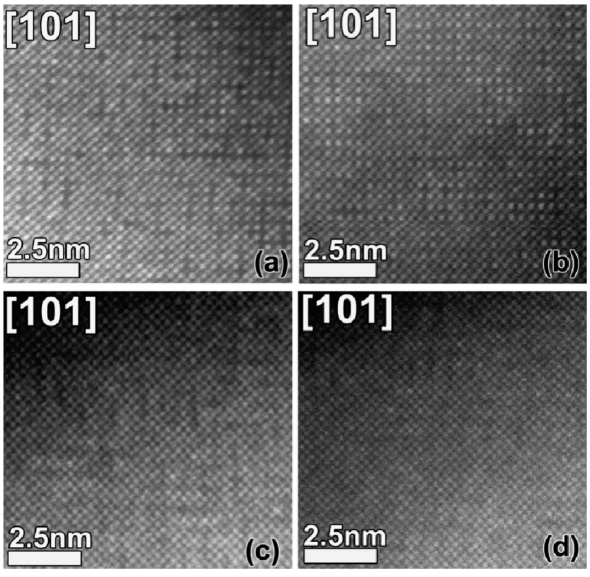

Figure 3. HAADF-STEM images of (a) $NaLaFeTaO_6$, (b) $NaLaMnTaO_6$, (c) $NaLaFeNbO_6$, and (d) $NaLaMnNbO_6$ along [101].

bright A-cation columns, and therefore we conclude that the local layered order occurs on the A-cation site. It should be pointed out that a layered order of Na vacancies would give the same appearance to the HAADF-STEM image; however, none of the techniques used in this study indicated such occurrence of Na vacancies.

Since layered A-cation order in the literature so far is always accompanied by rock salt-type order at the B-cation site, HAADF-STEM images along $\langle 101 \rangle_p$ zones were taken of $NaLaMnTaO_6$, a compound with a clear difference in Z between the B and B′ cations. This compound with B = Mn ($Z = 25$) and

dx.doi.org/10.1021/cm200226u |*Chem. Mater.* 2011, 23, 2398–2406

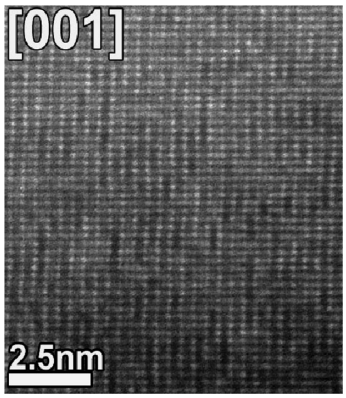

Figure 4. HAADF-STEM image along [001] of $NaLaMnTaO_6$, showing the absence of a chessboard ordered pattern in the brightest rows, thus the absence of rock salt-type order at the B-cation site.

B′ = Ta ($Z = 73$) should show a clear chessboard order of brighter and less bright dots in the HAADF-STEM images of the $\langle 101\rangle_p$ zones in the case of rock salt-type order of these B−B′ cations. A representative image along [001] of $NaLaMnTaO_6$ is shown in Figure 4 and it is clear that no such order is visible; therefore, the layered A-cation order in the current compounds is not accompanied by rock salt-type B-cation order. In this image the darker rows at the A-cation positions are also visible, similar to Figure 3.

It is clear from these images that the order is not long range; twinning and antiphase boundaries occur on a very local scale. The streaking of the first set of extra reflections originates from this local character of the order. The streaks are more pronounced in Figure 1d compared to those in Figure 1a; Figure 1b,c show an intermediate intensity of the streaking. On the HAADF-STEM images this corresponds to an increase in the amount of the A-cation order: Figure 3a (corresponding to Figure 1a, $NaLaFeTaO_6$) shows a more random distribution than Figure 3d; unfortunately, the smaller difference in average Z between the AA′ and the BB′ cation columns decreases the contrast in (c) and (d) of Figure 3, which is of course unrelated to the amount of order.

Taking into account the occurrence of local ordering of the A-cations, it is possible to determine the potential space groups with the systematic method specific for perovskites containing both tilted BX_6 and layered ordering of the A-cations established by Kishida et al.[25] It is only sensible to do this for the sample with negligible streaking and clear reflections, $NaLaFeTaO_6$, and even there the determined space group will not serve for further refinements, because of the large amount of twinning and antiphase boundaries, which makes the space group applicable to nanometer-sized domains only. For this determination, tilt series are taken from $\langle 111\rangle_p$ to the different $\langle 100\rangle_p$ zones lying within the tilting range of the TEM used (90° tilt range around one axis, 60° around the second axis). One such set of SAED patterns taken from a very thin area of $NaLaFeTaO_6$ is shown in Figure 5. To be able to refer in a clear manner to the paper by Kishida et al., the indices on Figure 5 are related to the perovskite parent structure, as indicated by the subscript "p" ($\mathbf{a}_p^* = \mathbf{a}^* + \mathbf{c}^*$, $\mathbf{b}_p^* = 2\mathbf{b}^*$, $\mathbf{c}_p^* = -\mathbf{a}^* + \mathbf{c}^*$). Cross-referencing with the table in Kishida et al. leaves for this set only one possible indexation, which is the one shown on the figure (Figure 5). Superstructure reflections observed in $[111]_p$ are assigned to the $1/2(oeo)_p$ type, assuming that the layered ordering of A-cations occurs

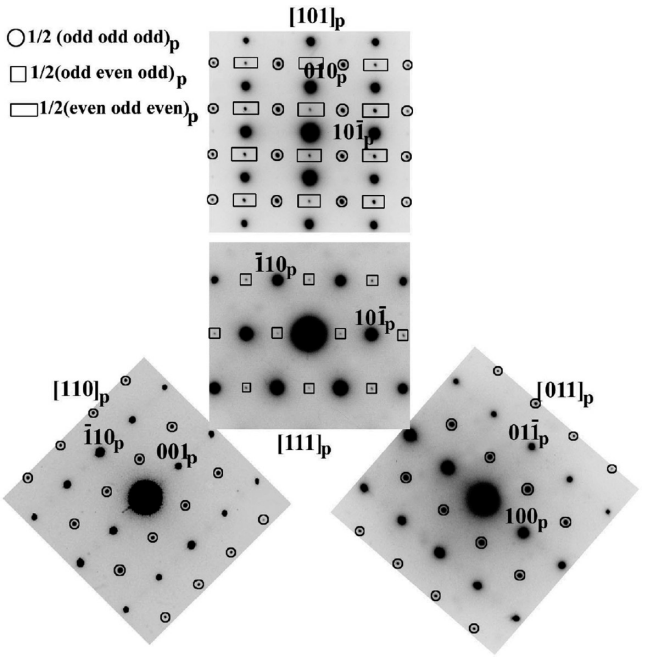

Figure 5. ED patterns taken from $NaLaFeTaO_6$ projected along the $[111]_p$, $[110]_p$, $[101]_p$, and $[011]_p$ directions. Indices with subscript p refer to the ideal perovskite structure.

along the b-axis of the ideal perovskite structure. In the $[101]_p$ there are two types of superstructure reflections indexed as those of types $1/2(eoe)_p$ and $1/2(ooo)_p$, while in $[011]_p$ and $[110]_p$ there is only one type of super-reflection indexed as $1/2(ooo)_p$. The possible space groups that are consistent with these extra reflections are $P2_1ma$, $P2/b$, and $Pmma$. The difference between them lies in the tilt system: $P2_1ma$ corresponds to $a^-B^+a^-$, $P2/b$ to $a^-B^-a^-$, and $Pmma$ to $a^-B^0a^-$, where the capital letter indicates the axis along which there is an ordered alternation of the A-cations. Eliminating any of these possibilities requires the performance of convergent beam electron diffraction (CBED), which would allow us to discover the presence of mirror planes. Unfortunately, CBED is not an option here since the nanoscale twinning can lead to the appearance of more mirror planes in the CBED patterns than there are in reality and therefore would not give any conclusive answers about the symmetry.

A simulated image for a model with layered A-cation order has been inserted in Figure 2; the model itself is shown in the bottom right corner. The model that was used has $a^-B^+a^-$; however, along this projection the different tilt systems $a^-B^+a^-$, $a^-B^-a^-$, and a^-B^0a will give the same image. The image was calculated for a focus value $f = -240$ Å and thickness $t = 117$ Å.

The reflections that correspond to the tilt system are strong on the SAED patterns, and appear also on the XRPD patterns and NPD patterns (following sections). The reflections corresponding to the layered order are streaked and due to local order only. The latter set is not distinguishable on the bulk X-ray or neutron powder diffraction patterns. Therefore, using the space group determined for the local order will be senseless for the refinement of the XRPD/NPD patterns. On the other hand, the refinement using XRPD or NPD will allow the determination of the correct tilt system. The three tilt systems that are possible according to the analysis of the electron diffraction patterns are $a^-b^+a^-$, $a^-b^-a^-$, and $a^-b^0a^-$, which in conventional settings correspond

dx.doi.org/10.1021/cm200226u |*Chem. Mater.* 2011, 23, 2398–2406

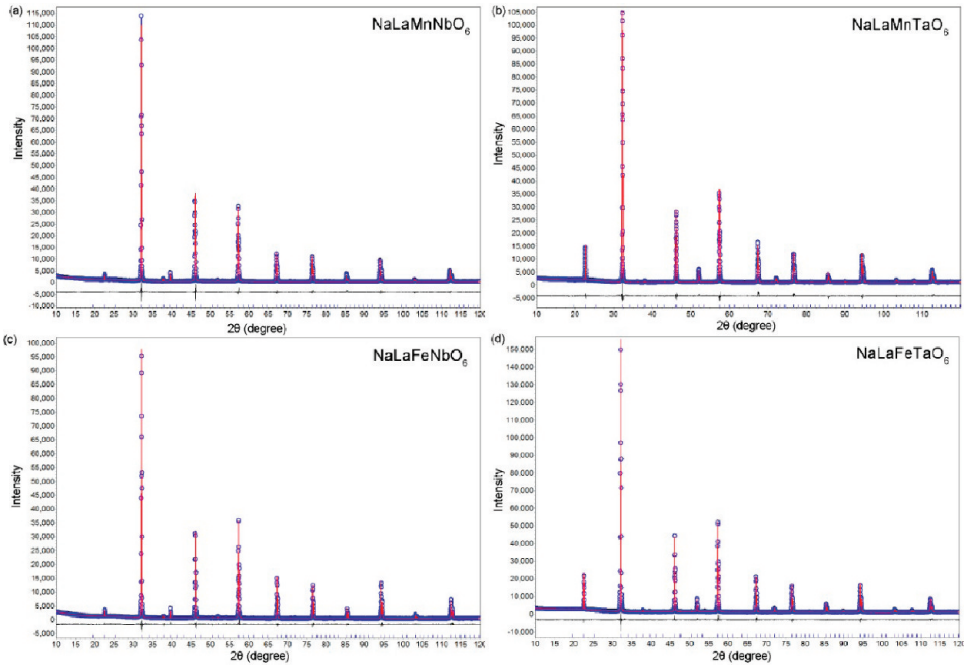

Figure 6. Rietveld refinement of the XRPD patterns for $NaLaBB'O_6$ (B = Mn, Fe; B′ = Nb, Ta). The blue symbol ○ represents the observed pattern and the red solid line is the calculated pattern; the blue marks below the diffraction patterns are the expected reflection positions, and the difference curve is also shown in black below the diffraction pattern.

Table 1. Crystallographic Data Obtained from XRPD Refinements of $NaLaBB'O_6$ (B = Mn, Fe; B′ = Nb, Ta)

	$NaLaMnNbO_6$	$NaLaMnTaO_6$	$NaLaFeNbO_6$	$NaLaFeTaO_6$
MW ($g \cdot mol^{-1}$)	405.75	493.79	406.66	494.70
space group	*Pnma*	*Pnma*	*Pnma*	*Pnma*
tilt system	$a^-b^+a^-$	$a^-b^+a^-$	$a^-b^+a^-$	$a^-b^+a^-$
a (Å)	5.569(1)	5.5580(1)	5.5609(2)	5.5608(2)
b (Å)	7.8774(1)	7.8533(1)	7.86637(9)	7.86121(9)
c (Å)	5.569(1)	5.5602(2)	5.5602(2)	5.5619(2)
V (Å^3)	244.34(9)	242.695(9)	243.22(4)	243.14(1)
Z	2			
radiation type	Cu *K*α λ = 1.5406 Å			
diffractometer	Bruker D8-Advance			
scan method	step/15s			
2θ values (deg)	$2\theta_{min}$ = 10, $2\theta_{max}$ = 120, $2\theta_{step}$ = 0.02			
ρ ($g \cdot m^{-3}$)	5.515	6.757	5.553	6.757
Rp (%)	4.96	3.84	4.79	3.35
Rwp (%)	6.63	5.07	6.65	4.47
gof	2.16	2.07	2.06	2.02

to the space groups *Pnma* ($a^-b^+a^-$), *C*2/*c* ($a^-b^-b^-$), and *Imma* ($a^-b^0a^-$) for the case of total cation disorder, such as this local order would be perceived by XRPD and NPD.

Rietveld Refinement of the X-ray and Neutron Powder Diffraction Data. Rietveld refinements of the XRPD data for the title compounds in Figure 6 show that the cell lattice sets are all $\sim\sqrt{2}a_p \times 2a_p \times \sqrt{2}a_p$. The refinements were carried out with space group *Pnma* (No. 62), which lead to very good convergence factors for all four compounds. All compounds appear to be phase-pure. Crystallographic data obtained from the refinement of the XRPD data is given in Table 1. Considering the similar cation radii on the A- and B-sites (see the footnote of Table 4), the very close cell volumes are understandable. The occupancy factors for the disordered cations on both the A- and B-sites were allowed to refine and converged to values close to 0.5.

Table 2. Unit Cell Parameters Obtained from Refinements of NPD Data

	$NaLaMnNbO_6$	$NaLaMnTaO_6$	$NaLaFeNbO_6$	$NaLaFeTaO_6$
a (Å)	5.5641(4)	5.5487(4)	5.5781(2)	5.5713(2)
b (Å)	7.8654(8)	7.8563(5)	7.8790(3)	7.8700(4)
c (Å)	5.5676(4)	5.5330(3)	5.5731(2)	5.5714(2)
V (Å^3)	243.66(2)	241.20(9)	244.94(4)	244.29(1)

Since the determination of the octahedral tilt system can sometimes be ambiguous from XRPD data alone, NPD data was collected on separate, larger sample batches which were synthesized in a manner similar to that of the samples used for the TEM and XRPD studies. As with the XRPD patterns, no supercell reflections corresponding to long-range cation ordering were observed. Rietveld refinements were performed with the three space groups suggested by ED, *Pnma*, *C*2/*c*, and *Imma*. In all four cases the refinements with *Pnma* provided a far superior fit (Figure S1 in the Supporting Information), confirming that this is the correct space group assignment. The unit cell parameters obtained from the NPD refinements are listed in Table 2, the atomic coordinates are listed in Table 3, and selected bond distances and angles are listed in Table 4. The results show similar B−O bond distances and B−O−B bond angles for all four compounds. The NPD patterns of the Fe compounds had small (~2%) Fe_2O_3 impurities, that were included as second phases. The Mn compounds had larger impurities of $LaMnO_3$, which were also included in the refinements. The observed impurity levels are consistent with the EDX results, which show that the Fe compounds form with B/B′ ratios which are

dx.doi.org/10.1021/cm200226u |*Chem. Mater.* 2011, 23, 2398–2406

Table 3. Atomic Coordinates and Displacement Parameters for $NaLaBB'O_6$ (B = Mn, Fe; B′ = Nb, Ta) from Room-Temperature NPD Rietveld Refinement

$NaLaMnNbO_6$	x	y	z	occ.	U_{eq}
La	0.0126(4)	0.25	−0.0034(7)	0.586	0.0159(3)
Na	0.0126(4)	0.25	−0.0034(7)	0.414	0.0159(3)
Mn	0	0	0.5	0.414	0.0011(2)
Nb	0	0	0.5	0.586	0.0011(2)
O1	0.5005(5)	0.25	0.0682(2)	1	0.0130(4)
O2	0.2686(2)	0.4740(1)	0.7337(4)	1	0.0139(2)
$NaLaMnTaO_6$	x	y	z	occ.	U_{eq}
La	0.0125(6)	0.25	−0.0051(7)	0.270	0.0190(3)
Na	0.0125(6)	0.25	−0.0051(7)	0.730	0.0190(3)
Mn	0	0	0.5	0.270	0.0055(3)
Ta	0	0	0.5	0.730	0.0055(3)
O1	0.4937(5)	0.25	0.0755(2)	1	0.0043(2)
O2	0.2710(3)	0.4779(1)	0.7257(3)	1	0.0100(2)
$NaLaFeNbO_6$	x	y	z	occ.	U_{eq}
La	0.0159(2)	0.25	0.0021(6)	0.474	0.0139(1)
Na	0.0159(2)	0.25	0.0021(6)	0.526	0.0139(1)
Fe	0	0	0.5	0.474	0.0065(1)
Nb	0	0	0.5	0.526	0.0065(1)
O1	0.4912(3)	0.25	0.0697(2)	1	0.0114(3)
O2	0.2740(2)	0.4710(1)	0.7250(2)	1	0.0094(1)
$NaLaFeTaO_6$	x	y	z	occ.	U_{eq}
La	0.0180(3)	0.25	0.0046(5)	0.470(1)	0.0119(2)
Na	0.0180(3)	0.25	0.0046(5)	0.530(1)	0.0119(2)
Fe	0	0	0.5	0.482(1)	0.0052(1)
Ta	0	0	0.5	0.518(1)	0.0052(1)
O1	0.4879(3)	0.25	0.0786(2)	1	0.0089(3)
O2	0.2726(2)	0.4719(1)	0.7233(2)	1	0.0072(1)

close to 1:1, while the Mn compounds tend to be slightly deficient in Mn.

Refinements of the Local Structure from the Pair Distribution Function. The pair distribution function (PDF) method allows the structure of a material to be probed at different length scales. PDFs derived from X-ray and neutron total scattering data were used to confirm that the short-range layered ordering observed by TEM is indeed associated with the A-site cations and to search for other local distortions that may be present. Various models were refined against the $G(r)$ functions at different length scales to determine the correlation lengths of the local distortions.

The initial fittings of the X-ray PDFs were done with the long-range average structures (complete cation disorder) as starting models. During the refinements the atoms were allowed to move within the constraints of *Pnma* symmetry. Refinements were done over r ranges of 1−10, 10−20, and 20−40 Å (Figure S2). The results were similar for all four compounds. The average long-range structures were able to provide excellent fits to the $G(r)$'s in the r ranges of 10−20 and 20−40 Å, showing that any deviations from the average structures are very short range. However, the average structures were not able to model the $G(r)$'s in the r range of 1−10 Å, which was an indication

Table 4. Selected Bond Distances (Å) and Angles (deg) in $NaLaBB'O_6$ (B = Mn, Fe; B′ = Nb, Ta)

	$NaLaMnNbO_6$	$NaLaMnTaO_6$	$NaLaFeNbO_6$	$NaLaFeTaO_6$
La/Na−O (Å)	2.424(4)	2.379(4)	2.391(4)	2.328(3)
	2.567(3) × 2	2.548(3) × 2	2.540(2) × 2	2.556(2) × 2
	2.697(3) × 2	2.707(4)	2.678(2)	2.650(2)
	2.744(4)	2.735(3) × 2	2.737(2) × 2	2.742(2) × 2
	2.818(3) × 2	2.765(3) × 2	2.784(2) × 2	2.763(2) × 2
	2.877(4)	2.913(4)	2.951(2)	2.982(2)
	3.069(3) × 2	3.071(3) × 2	3.125(2) × 2	3.1158(2) × 2
	3.145(4)	3.158(4)	3.190(2)	3.254(3)
⟨A−O⟩ (Å)	2.791	2.783	2.798	2.797
B−O (Å)	1.974(2) × 2	1.962(2) × 2	1.990(1) × 2	1.976(1) × 2
	1.992(2) × 2	1.987(2) × 2	1.998(1) × 2	2.007(1) × 2
	2.003(1) × 2	2.008(1) × 2	2.008(1) × 2	2.017(1) × 2
⟨B−O⟩ (Å)	1.990	1.986	1.999	2.000
t1 factor[a]	0.99	0.99	0.99	0.99
t2 factor[b]	0.98	0.98	0.98	0.98
B−O1−B (deg)	158.15(3)	155.90(2)	157.52(1)	154.61(1)
B−O2−B (deg)	165.71(8)	165.56(8)	162.72(5)	163.02(6)

[a] t_1 factor = $\langle A-O\rangle/\sqrt{2}\,\langle B-O\rangle$. [b] t_2 factor = $(\langle R_A\rangle + R_O)/\sqrt{2}(\langle R_B\rangle + R_O)$; R_{O2-} = 1.40 Å, R_{La3+} = 1.36 Å, R_{Na+} = 1.39 Å, R_{Mn3+} = 0.58 Å, R_{Fe3+} = 0.55 Å, R_{Nb5+} = 0.64 Å, R_{Ta5+} = 0.64 Å.

that short-range deviations from the average structure are present.

In an attempt to fit the low r regions of the PDFs, the *Pnma* models were modified to include either layered A-site ordering, layered B-site ordering, or both. Surprisingly, none of these models were able to provide any significant improvement to the fit. The most poorly fit regions of the X-ray PDFs are the peaks at ∼3.45 Å (Figure 7), which correspond to the nearest neighbor A-site cation to B-site cation distances. The experimental peaks appear at slightly higher r values than are predicted by the average structures. A possible explanation for this observation could be that the Nb/Ta atoms lie closer to the Na atoms than to the La atoms. Since the intensity of a point in $G(r)$ is proportional to the number of interatomic distances at a given r and also the product of the scattering power of the atoms in the pair, the (Nb/Ta)−La distances make the strongest contribution to this peak. Longer (Nb/Ta)−La and shorter (Nb/Ta)−Na distances would make the peak shift toward higher r, with a shoulder on the low r side from the (Mn/Fe)−(Na/La) and (Nb/Ta)−Na distances. This matches what is observed in the experimental $G(r)$. Such out-of-center displacements are common for highly charged d^0 transition metals such as Nb and Ta, which are well-known to undergo SOJT distortions. SOJT distortions have been observed in the long-range average structures of several other $AA'BB'O_6$ perovskites, which have both rock-salt ordering of B/B′ and layered ordering of A/A′.[16] In these compounds the d^0 cations displace toward the Na layer and away from the Ln^{3+} layer in order to relieve a bonding instability that is created by the layered ordering of A-site cations. Assuming that something similar is occurring in the title compounds, but only on a local level, new models were constructed which have a layered ordering of the Na and La cations and also allow the Nb or Ta cations to displace in the direction perpendicular to the layered A-site ordering. Refinements using these models were able to provide good fits to the low r regions of the X-ray PDFs (Figure 7) and it was observed that the Nb/Ta ions did indeed displace toward Na and away from La.

Refinements of the neutron PDFs gave similar results. Fits with the long-range average structures were able to account for all

dx.doi.org/10.1021/cm200226u |*Chem. Mater.* 2011, 23, 2398–2406

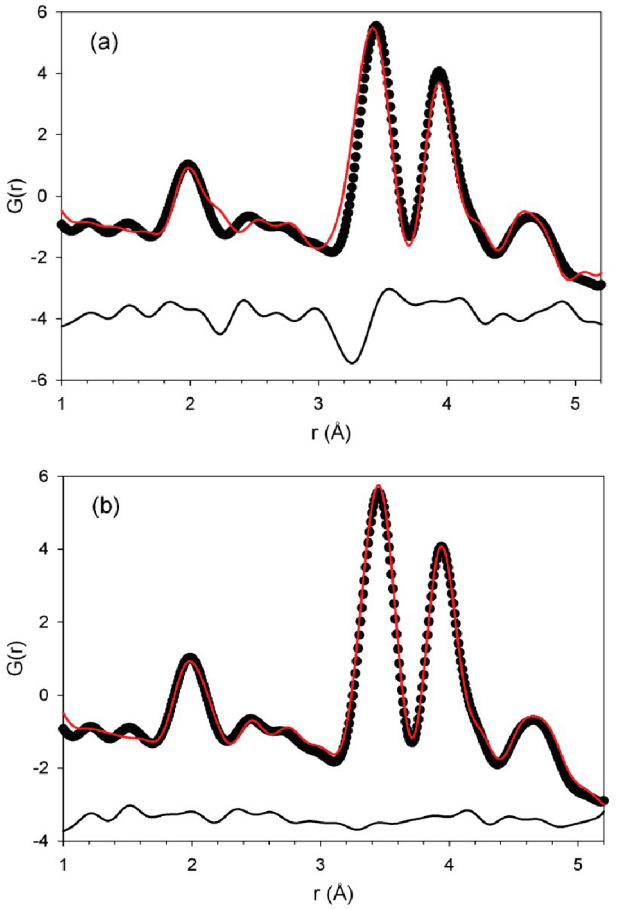

Figure 7. Refinements of the low r region of the X-ray $G(r)$ of $NaLaFeTaO_6$ showing the fit with the average structural model (a) and the model that includes layered A-site ordering and SOJT distortions of the Ta cations (b). The black circles show the experimental $G(r)$, the red line is the calculated fit, and the black line is the difference curve.

of the features of the $G(r)$'s at high r values. For the two Fe-containing compounds the fit to the peak ~3.45 Å was not obviously poor when using the average structure as a model. Morever, when a model with layered A-site ordering and SOJT displacements of the Nb/Ta atoms were imposed, the fit did not change significantly. From this result it can be concluded that because of the similar neutron scattering powers of the elements in these compounds, the $G(r)$ is not sensitive to the presence or absence of these features. Because of the negative scattering length of Mn, the PDFs of the Mn-containing compounds are highly sensitive to these features. The regions around ~3.45 Å are poorly fit by the average structures, but can be well modeled with the same models that were used to successfully fit the low r regions of the X-ray PDFs.

These observations provide important new insight into the nature of A-site cation ordering in perovskites. It has been previously shown that there are two criteria necessary to obtain a layered arrangement of A-site cations: (1) a rock-salt ordering of two B-site cations and (2) a SOJT cation on one of the B-sites. The present results show that when SOJT cations are present, but there is a disordered arrangement of B-site cations, layered A-site ordering can still occur on a local level. It appears that the ordering of B-site cations is not a necessary criterion for layered

Table 5. r_w of the Final Fit, Local Lattice Parameters, and Magnitude of the Displacement of the d^0 B′ Cation (Å) for the $NaLaBB'O_6$ (B = Mn, Fe; B′ = Nb, Ta) Compounds as Derived from the X-ray PDF Analysis

	$NaLaFeTaO_6$	$NaLaMnNbO_6$	$NaLaFeNbO_6$	$NaLaMnTaO_6$
r_w	9.32	11.32	12.22	19.09
a	5.532	5.345	5.572	5.359
b	7.917	8.053	7.887	8.040
c	5.576	5.701	5.511	5.743
B′ displacement	0.118	0.105	0.142	0.077

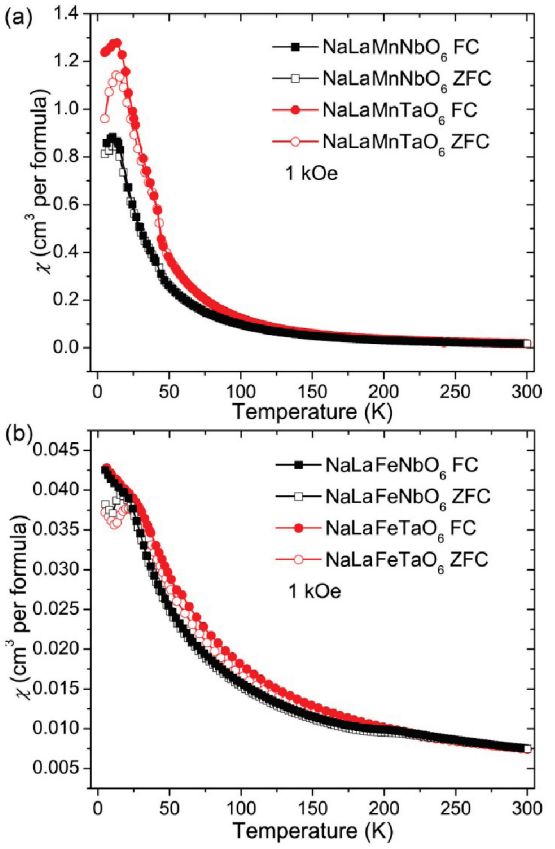

Figure 8. Magnetic susceptibilities χ at 1 kOe field at ZFC and FC conditions for $NaLaBB'O_6$: (a) B = Mn, B′ = Nb, Ta; (b) B = Fe, B′ = Nb, Ta.

A-site ordering, but is necessary for that ordering to be long range.

The unit cell metrics of the average structures are all very close to cubic. The unit cell dimensions obtained from the refinements of the low r regions of the PDFs show a greater orthorhombic distortion (Table 5). It is worth noting that the two compounds that contain Mn^{3+} have a much greater local orthorhombic distortion than those that contain Fe^{3+}. These distortions can be attributed to FOJT distortions of the Mn^{3+} ions. Although there are no indications of pronounced cooperative Jahn−Teller distortions in the average structures, it appears that such distortions are locally present for both Mn compounds.

Magnetism. The Mn and Fe compounds show contrasting magnetic behaviors. The zero-field-cooled and field-cooled (ZFC-FC) temperature-dependent magnetic susceptibilities for $NaLaBB'O_6$ (B = Mn, Fe; B′ = Nb, Ta) under a 1 kOe field are

dx.doi.org/10.1021/cm200226u |*Chem. Mater.* 2011, 23, 2398–2406

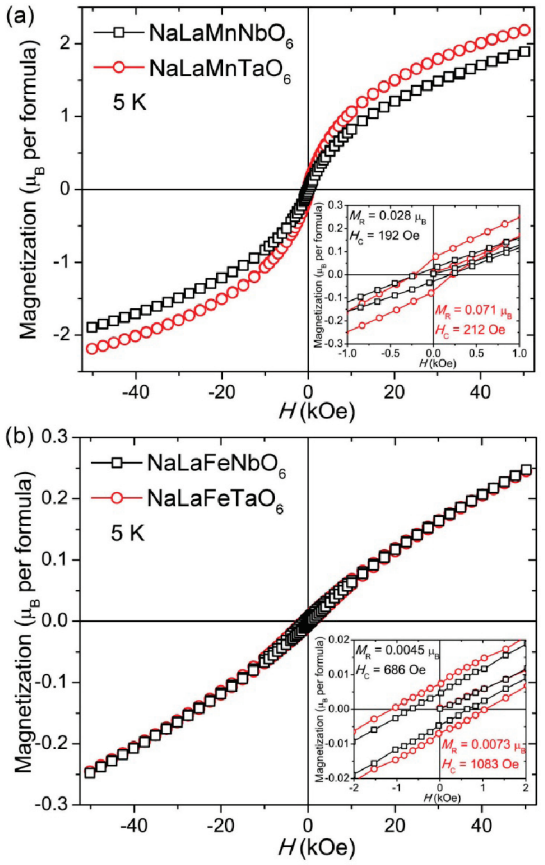

Figure 9. Field dependence of the magnetization plots at 5 K. The insets are the enlargements of the low field region.

shown in Figure 8. The susceptibility values of the Mn compounds are much larger than those of the Fe compounds. Indeed, the Curie−Weiss fit of the high-temperature data gives positive θ values for the Mn compounds (85 K for $NaLaMnNbO_6$ and 97 K for $NaLaMnTaO_6$) and negative values for the Fe compounds (−132 K for $NaLaMnNbO_6$ and −86 K for $NaLaMnTaO_6$), respectively (Figures S3 and S4 in the Supporting Information). Further, there is a small anomaly in the susceptibility curve of Mn compounds at ∼45 K, which may be due to a small impurity of Mn_3O_4. In the susceptibility plot of $NaLaFeNbO_6$, a broad cusp at ∼200 K cannot be explained as yet. Nevertheless, the main magnetic features of the title compounds are clear: the magnetic interactions in the Mn compounds are ferromagnetic (FM), and antiferromagnetic (AFM) for Fe compounds. This is further confirmed by the field-dependent magnetization plots in Figure 9: at 5 K and 5 T, the Mn compounds reach ∼50% of the theoretical saturation of Mn^{3+} (4 μ_B for $S = 2$), while the magnetizations of the Fe compounds are just 5% of the theoretical saturation value (5 μ_B assuming $S = 5/2$). All four compounds show a small magnetic remnant and coercive field (see the insets of Figure 9), consistent with the divergence of the ZFC-FC curves at low temperatures (Figure 8). We attribute the divergence of the ZFC-FC to glassy components, which are not surprising, given the extensive structural disorder. The magnetization in Mn compounds are relatively high, considering the absence of long-range magnetic order; this is attributed to the presence of ferromagnetic clusters in the Mn compounds, which is not uncommon for polycrystalline oxide materials. The magnetism of $A_2BB'O_6$ (A = Ca, Sr; B = Mn, Fe; B′ = Ta, Nb) is a good reference for the compounds studied here: it is found that the Mn compounds of B^{3+}/B'^{5+} double perovksites are FM, while the Fe analogues are basically AFM.[26−28] Thus, the short-range order of Na and La in the A-site has no significant effect on the magnetism, relative to the perovskites with A = Ca, Sr in similar double perovskites.

Neutron powder diffraction patterns were taken at 4 K to look for signs of magnetic ordering. The low-temperature NPD patterns do not contain any new peaks of magnetic origin and the peak intensities are nearly identical to those of the room-temperature NPD patterns. This is consistent with the absence of long-range magnetic ordering in these samples.

CONCLUSIONS

Four new perovskite compounds, $NaLaMnNbO_6$, $NaLaMnTaO_6$, $NaLaFeNbO_6$, and $NaLaFeTaO_6$ have been prepared. They all crystallize in space group *Pnma*, corresponding to the $a^-b^+a^-$ tilt system. While none of the compounds show any long-range cation order, short-range A-site layered ordering was observed in all four compositions. This is accompanied by second-order Jahn−Teller displacements of the Nb^{5+} and Ta^{5+} cations, which also lack any long-range correlations. One of the most notable findings of this study is the observation of layered A-site ordering without the rock salt B-site ordering that is typically found to accompany it. Thus, it can be concluded that B-site ordering is necessary for the layered A-site ordering to be long range, but such ordering can still occur locally even in its absence. The two Fe-containing compounds have antiferromagnetic interactions, while the two Mn-containing compounds have ferromagnetic interactions. However, no long-range magnetic ordering is observed in any of the compounds above 4 K.

ASSOCIATED CONTENT

Supporting Information. This information is available free of charge via the Internet at http://pubs.acs.org/.

AUTHOR INFORMATION

Corresponding Author

*Telephone: 732-445-3277. E-mail: martha@rutchem.rutgers.edu.

Author Contributions

⊥W.D. and T.Y. are co-first authors.

ACKNOWLEDGMENT

This work was partially supported by NSF-DMR 0541911 grant (M.G., T.Y.). W.D., J.H., and G.V.T. acknowledge financial support from the European Union under the Framework 6 program under a contract for an Integrated Infrastructure Initiative, Reference 026019 ESTEEM. This work has benefited from the use of HIPD at the Lujan Center at Los Alamos Neutron Science Center, funded by DOE Office of Basic Energy Sciences. Los Alamos National Laboratory is operated by Los Alamos National Security LLC under DOE Contract DE-AC52 06NA25396. Use of the Advanced Photon Source at Argonne National Laboratory was supported by the U.S. Department of Energy, Office of Science, Office of Basic Energy Sciences, under Contract No. DE-AC02-06CH11357.

REFERENCES

(1) Cava, R. J.; Batlogg, B.; van Dover, R. B.; Krajewski, J. J.; Waszczak, J. V.; Fleming, R. M.; Peck, W. F.; Rupp, L. W.; Marsh, P.; James, C. W. P.; Schneemeyer, L. F. *Nature* **1990**, *345*, 602–604.

(2) Newnham, R. E.; Ruschau, G. R. *J. Am. Ceram. Soc.* **1991**, *74*, 463–480.

(3) Davies, P. K. *Curr. Opin. Solid State Mater. Sci.* **1999**, *4*, 467–471.

(4) Goodenough, J. B. *Rep. Prog. Phys.* **2004**, *67*, 1915–1993.

(5) Lufaso, M. W.; Barnes, P. W.; Woodward, P. M. *Acta Crystallogr., Sect. B* **2006**, *62*, 397–410.

(6) Anderson, M. T.; Greenwood, K. B.; Taylor, G. A.; Poeppelmeier, K. R. *Prog. Solid State Chem.* **1993**, *22*, 197–233.

(7) Howard, C. J.; Kennedy, B. J.; Woodward, P. M. *Acta Crystallogr., Sect. B* **2003**, *59*, 463–471.

(8) Davies, P. K.; Wu, H.; Borisevich, A. Y.; Molodetsky, I. E.; Farber, L. *Annu. Rev. Mater. Res.* **2009**, *38*, 369–401.

(9) Anderson, M. T.; Poeppelmeier, K. R. *Chem. Mater.* **1991**, *3*, 476–482.

(10) Anderson, M. T.; Poeppelmeier, K. R.; Gramsch, S. A.; Burdett, J. K. *J. Solid State Chem.* **1993**, *102*, 164–172.

(11) Ducau, M.; Suh, K. S.; Senegas, J.; Darriet, J. *Mater. Res. Bull.* **1992**, *27*, 1115–1123.

(12) Torres-Pardo, A.; Krumeich, F.; González-Calbet, J. M.; García-González, E. *J. Am. Chem. Soc.* **2010**, *132*, 9943–9949.

(13) King, G.; Wayman, L. M.; Woodward, P. M. *J. Solid State Chem.* **2009**, *182*, 1319–1325.

(14) Knapp, M. C.; Woodward, P. M. *J. Solid State Chem.* **2006**, *179*, 1079–1085.

(15) King, G.; Thimmaiah, S.; Dwivedi, A.; Woodward, P. M. *Chem. Mater.* **2007**, *19*, 6451–6458.

(16) King, G.; Woodward, P. M. *J. Mater. Chem.* **2010**, *20*, 5785–5796.

(17) TOPAS V2.1: General Profile and Structure Analysis Software for Powder Diffraction Data; Bruker AXS: Karlsruhe, Germany, 2000.

(18) Hammersley, A. P. ESRF Internal Report, ESRF98HA01T, FIT2D V9.129 Reference Manual V3.1, 1998.

(19) Hammersley, A. P.; Svensson, S. O.; Hanfland, M.; Fitch, A. N.; Hausermann, D. *High Pressure Res.* **1996**, *14*, 235–248.

(20) Qiu, X.; Thompson, J. W.; Billinge, S. J. L. *J. Appl. Crystallogr.* **2004**, *37*, 678.

(21) Toby, B. H. *J. Appl. Crystallogr.* **2001**, *34*, 210–213.

(22) Larson, A. C.; Von Dreele, R. B. *General Structure Analysis System (GSAS)*; Los Alamos National Laboratory Report LAUR; Los Alamos National Laboratory: Los Alamos, NM, 2004; Vol. 86, p 748.

(23) Peterson, P. F.; Gutmann, M.; Proffen, Th.; Billinge, S. J. L. *J. Appl. Crystallogr.* **2000**, *33*, 1192.

(24) Farrow, C. L.; Juhas, P.; Liu, J. W.; Bryndin, D.; Bozin, E. S.; Bloch, J.; Proffen, Th.; Billinge, S. J. L. *J. Phys.: Condens. Matter* **2007**, *19*, 335219.

(25) Kishida, K.; Goto, K.; Inui, H. *Acta Crystallogr., Sect. B* **2009**, *65*, 405–415.

(26) Battle, P. D.; Gibb, T. C.; Herod, A. J.; Kim, S. H.; Munns, P. H. *J. Mater. Chem.* **1995**, *5*, 865–870.

(27) Cussen, E. J.; Vente, J. F.; Battle, P. D.; Gibb, T. C. *J. Mater. Chem.* **1997**, *7*, 459–463.

(28) Mandal, T. K.; Poltavets, V. V.; Croft, M.; Greenblatt, M. *J. Solid State Chem.* **2008**, *181*, 2325–2331.